Journal of Power Sources 199 (2012) 270–277

Contents lists available at SciVerse ScienceDirect

Journal of Power Sources

journal homepage: www.elsevier.com/locate/jpowsour

Binder free, porous and nanostructured Co_3O_4 anode for Li-ion batteries from solution precursor plasma deposition

Raghavender Tummala, Ramesh K. Guduru*, Pravansu S. Mohanty

Department of Mechanical Engineering, University of Michigan, Dearborn, MI 48128, United States

ARTICLE INFO

Article history:
Received 17 September 2011
Received in revised form 12 October 2011
Accepted 13 October 2011
Available online 20 October 2011

Keywords:
Li-ion batteries
Cobalt oxide
Anode
Solution precursor
Plasma deposition
Cyclability
Specific capacity

ABSTRACT

Increasing demand for high energy density in Li-ion batteries has fueled intensive efforts for the search of high specific capacity anode materials to replace the carbon anodes. Among transition metal oxides, nanostructured Cobalt oxide (Co_3O_4) was found to be one of the better anode materials for Li-ion batteries. However, the processing routes employed so far have been able to produce different kinds of nanostructured Co_3O_4 powders, which then require further processing to obtain battery electrodes. Here, we propose a single step and industrial scale solution precursor plasma technique to develop nanostructured, porous and flexible Co_3O_4 electrodes directly on current collectors. In this process, an aqueous solution precursor comprising of cobalt acetate is fed into a plasma plume to form nanostructured Co_3O_4 particles, which are then deposited on a current collector. These electrodes are binder and carbon free, and their microstructures revealed nano particulate structure with porosity. Phase, crystallinity and microstructures of the Co_3O_4 films were investigated by X-ray diffraction, Differential scanning calorimetry–Thermogravimetry (DSC–TGA), Scanning electron microscopy (SEM) and Transmission electron microscopy (TEM). Electrochemical characterization indicated an average cell voltage of ~1.0–1.25 V against Li electrode with specific discharge capacities close to the theoretical value (~890 mAhr g^{-1}).

1. Introduction

Rechargeable Li-ion batteries are very promising power sources for different applications ranging from small scale microelectronic devices to hybrid electric vehicles because of high energy density and long cycle life [1–3]. But, their energy density is limited by specific capacity of the electrodes used in the cell. Carbon anodes have been in use in Li-ion batteries since their commercialization because of very low potential of carbon with respect to the cathode materials. However, limited specific capacity of carbon (~372 mAhr g^{-1}), and increasing global demand for high energy density Li-ion batteries for automobile and other large scale applications has been driving the researchers to search for alternative anode materials. Although different material systems have been proposed for anodes [4], the most important challenge in all of them is maintaining the structural integrity over many charge–discharge cycles. Also, the life span of these anode materials is limited due to alloying with Li [4–10]. In the year of 2000, discovery by Tarascon et al. [11] has opened up new opportunities for transition metal oxides as anode materials in Li-ion batteries. However, operating mechanism of these materials is quite different from the regular Li-ion intercalation mechanism. Among various transition metal oxides, Co_3O_4 has attracted more attention because of high capacity (~890 mAhr g^{-1}) and cyclability. The electrochemical interaction of Co_3O_4 with Li (or Li based cathode compounds) follows the reaction shown below [12], and the Li_2O formed in this process behaves as an electrochemically active material in the reverse reaction.

$$Co_3O_4 + 8Li^+ + 8e^- \rightleftarrows 3Co + 4Li_2O \quad (1)$$

Usually, nanostructured electrodes with porosity are desired for enhanced electrochemical reaction kinetics as they provide huge surface area, reduced mass and charge diffusion distances along with added freedom for volume change. There has been extensive research going on to develop nanostructured Co_3O_4 anodes. Different processing techniques, including wet chemical processes [13–18], solid state syntheses [19], hydrothermal, vapor based and microwave methods [20–24], have been adopted to tailor the structures of Co_3O_4 and thereby the electrochemical properties. But, most of these techniques need either longer processing times or expensive techniques to synthesize the nanostructured powders of Co_3O_4. Consequently these powders require multi-step processing, such as mixing with binder, solvent and additives, then coating machines to spread them on metal foils, and calendaring the coated foils to get uniform thickness etc. [25]. Thus the electrode and battery manufacturing process becomes very time intensive and

* Corresponding author. Tel.: +1 313 583 6705; fax: +1 313 593 3851.
E-mail addresses: rkguduru@umich.edu, rameshkumarg5@yahoo.com (R.K. Guduru).

0378-7753/$ – see front matter © 2011 Elsevier B.V. All rights reserved.
doi:10.1016/j.jpowsour.2011.10.048

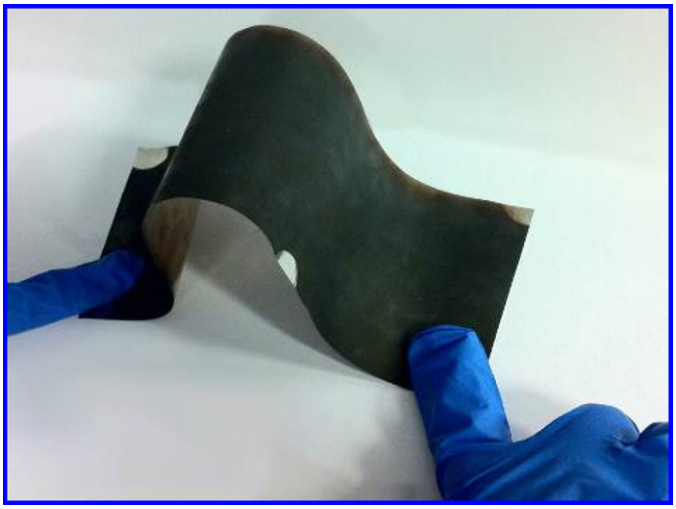

Fig. 1. Solution precursor plasma deposited flexible Co_3O_4 electrode on a stainless steel sheet (SS304) current collector.

expensive. On the other hand, few research groups [9,16,26–32] have concentrated on developing self supported nanowire arrays of anode materials (e.g., Co_3O_4, Si etc.) directly on a current collector with or without template assistance. But, the synthesis techniques employed by these groups were again time consuming and less attractive for large scale production. Therefore, manufacturing of nanostructured anodes along with cost reduction is very vital from the commercial application point of view.

Here, we report rapid processing of Co_3O_4 electrodes using an industrial scale solution precursor plasma deposition route. This approach makes use of a solution precursor comprising water dissolved cobalt acetate to synthesize bulk scale, nanostructured, porous and flexible Co_3O_4 electrodes (see Fig. 1) in ambient conditions. It is also capable of developing electrode films/coatings on complex shapes. During the synthesis process, solution precursor is fed through an atomizer into the plasma plume, which will then undergo accelerated thermo-chemical conversion to form fine Co_3O_4 phase particulates. Thus converted Co_3O_4 particles will propel toward the substrate/current collector to form electrode films (thickness ~10–15 μm). Characterization of these anodes in terms of microstructure and electrochemical performance are discussed in the forthcoming sections.

2. Experimental procedure

Solution precursor was prepared by dissolving 0.2 mol of cobalt acetate tetrahydrate (98% pure, Alfa Aesar, USA) in 1000 ml of deionized water. For complete dissolution of cobalt salt, solution was stirred for half an hour using a magnetic stirrer. A modified 100HE plasma gun (Progressive Technologies Inc., Grand Rapids, MI, USA) was used for depositing Co_3O_4 films on a 25 μm thick stainless steel (304 SS, McMaster Carr Inc., USA) sheet (current collector). An axial liquid atomizer was used to feed the solution precursor into the plasma plume. Spray parameters employed for deposition of Co_3O_4 films are shown in Table 1.

Phase and crystallinity of all the materials were determined from X-ray diffraction (XRD) studies conducted using a Rigaku Miniflex X-ray diffraction machine with a Cu K_α radiation (λ = 1.5402 Å). DSC–TGA experiments were performed on SDT Q600 by heating the samples from room temperature to 1200 °C in air with a ramp rate of 20 °C min^{-1}. Surface and bulk microstructures were examined using SEM (Hitachi 2600-N) and TEM (Hitachi HT 7700), respectively. The samples for TEM studies were prepared following drop-cast method using scraped powders of Co_3O_4 films.

Table 1
Solution precursor plasma spray process parameters.

Parameter	Value
Power (kW)	75
Voltage (V)	235
Current (A)	230
Primary gas ($m^3\ h^{-1}$) (argon)	4.89
Secondary gas ($m^3\ h^{-1}$)Nitrogen and hydrogen	2.6 and 2.96
Standoff distance (mm)	115
Feed rate (ml min^{-1}) (solution precursor)	45
Atomizing gas (kPa) (compressed air)	182.36
Cooling gas (kPa) (compressed air)	344.73
Material deposition density	~3.8–4 mg cm^{-2}

Electrochemical characterization was done on Biologic VMP3 analyzer using coin cell assembly. Co_3O_4 half cells were prepared in a glove box (Ar atmosphere) with electrolyte (1.5 M $LiPF_6$ dissolved in Ethylene carbonate (EC):Dimethyl carbonate (DMC) – 1:2 solution), *Celgard 2500*™ separator and Li counter electrode. All the half cells were assembled in 20 mm diameter coin cells (CR2032) and then crimped. Testing of the coin cells was done by placing them in a stainless steel cell (MTI Corporation).

3. Results and discussion

3.1. Synthesis and phase analysis

Fig. 2 shows a schematic of solution precursor plasma deposition technique used for the synthesis of Co_3O_4 anodes in the present research. As shown in Fig. 2, the solution precursor is atomized by compressed air in the atomizer and enters into plasma plume as fine droplets. Then the high temperatures of plasma plume accelerate the thermo-chemical conversion of the solution precursor droplets into Co_3O_4, which eventually deposit on the stainless steel (SS304) substrate, i.e., current collector. Fig. 3 shows an SEM image of the Co_3O_4 anode developed following this approach. Crystallinity and phase structure of the as-deposited films were determined by X-ray diffraction studies, which are shown in Fig. 4 along with the X-ray diffraction pattern of commercial Co_3O_4 powders. These studies confirm cubic phase and polycrystalline nature of the Co_3O_4 anode films. It is evident from the literature [33–35] that formation of Co_3O_4 phase during thermo-chemical conversion of cobalt acetate tetrahydrate (CATH) could be dependent on several factors; for example, the atmospheric conditions employed. According to Mohamed et al. [33], dissociation of CATH at high temperatures (>400 °C), and especially in presence of air, can result in the formation of Co_3O_4 phase. Otherwise, it could lead to the formation of CoO or metallic Co phases in N_2 and H_2 atmospheres, respectively [34,35]. In the plasma deposition approach, the thermo-chemical conversion of solution precursor and deposition of the anode films is usually carried out in ambient air, and therefore, formation of Co_3O_4 is quite plausible. However, the extent of thermo-chemical conversion of solution precursor droplets is dependent on several process parameters; such as the temperature of the plasma plume, size/mass of the atomized droplets, time of retention for the droplets within the plasma plume, and/or velocity of the droplet injection. In fact, all these parameters are interdependent, because the velocity of injection can limit the droplet size in thermo-chemical conversion process by affecting the total time of retention in the plasma plume. Small droplet size is preferred for rapid thermo-chemical conversion, and the size of the droplets during atomization process can be tailored by varying the pressure of compressed air as well as the flow rate of the solution precursor. But, the pressure of atomization gas (compressed air) can also act together with the velocity of the plasma jet and control the time of retention. Hence, these three parameters are very critical to achieve

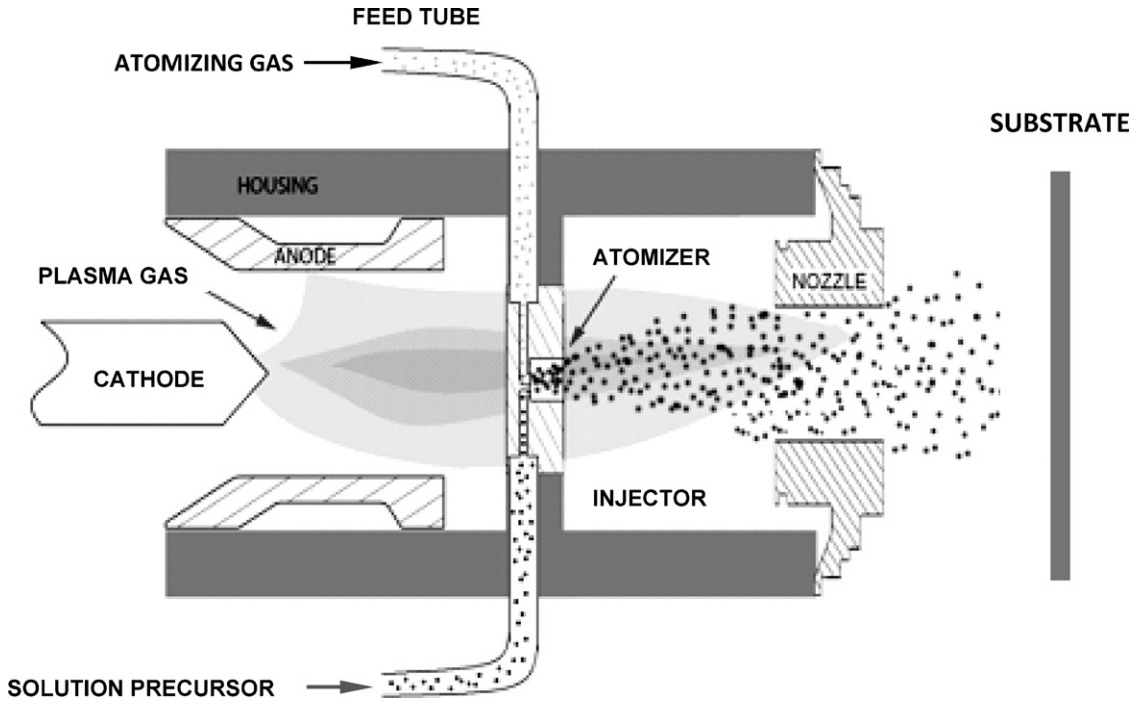

Fig. 2. Schematic of solution precursor plasma deposition technique.

maximum conversion of the solution precursor before depositing on the substrate/charge collector. Detailed discussion of solution precursor spray deposition can be found elsewhere [36,37].

To understand the thermo-chemical conversion of solution precursor in the plasma splume, we conducted DSC–TGA studies on the solution precursor and these are shown in Fig. 5. The endothermic peak around 100 °C in DSC heat flow curve and associated weight loss in TGA data indicate evaporation of water molecules. However, further endothermic reaction above 100 °C with very little weight loss may be due to dissociation of CATH. Literature [33–35] suggests that dissociation of CATH occurs in different stages with increasing the temperature. Mohamed et al. [33] showed initial conversion of CATH into monohydrate and further dehydration with increasing temperatures above 200 °C. All the stages of dehydration are usually associated with very small amounts of weight loss and endothermic reactions. Although, the endothermic reactions in the present data are not clearly discernible in the DSC heat flow curve, but the TGA graph shows gradual weight loss due to the dehydration of CATH. According to Mohamed et al. [33] the volatile decomposition products of CATH were acetone, acetic acid, acetaldehyde and CO_2 and the exothermic peak around 360 °C could be because of the oxidation of non-volatile dissociation products, such as formation of Co_3O_4 phase. However, with further increase in the temperature there was an endothermic peak around 900 °C and it must be due to conversion of Co_3O_4 into CoO with a slight amount of oxygen loss, which is also apparent from the weight loss in TGA curve. Therefore, we believe that the solution precursor will undergo similar thermo-chemical conversion process when the atomized droplets of solution precursor are exposed to the plasma plume, but at rapid rates because of high temperatures of the plasma (~10,000–12,000 °C). In the early stages of conversion process, a huge volume change in the size of solution precursor droplets can also be expected due to evaporation of water molecules. But, as the particles exit the plasma plume and propel toward the substrate in the ambient atmosphere, their

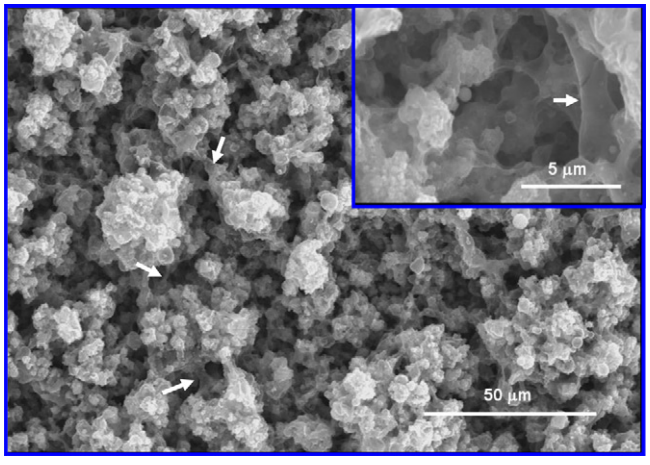

Fig. 3. Co_3O_4 anode films synthesized using solution precursor plasma deposition technique (inset – zoom in view).

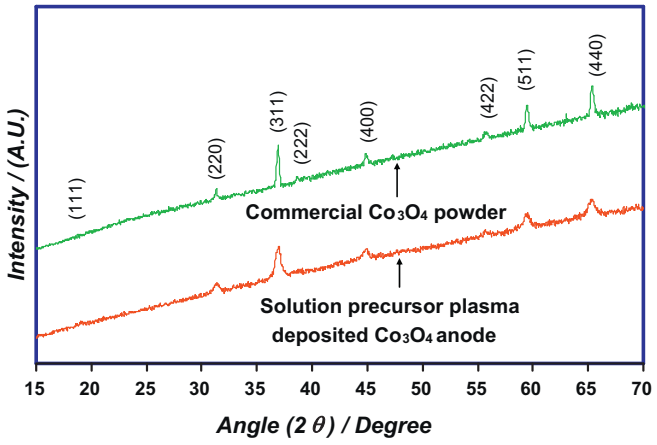

Fig. 4. X-ray diffraction patterns for solution precursor plasma deposited Co_3O_4 anode and commercial Co_3O_4 powders.

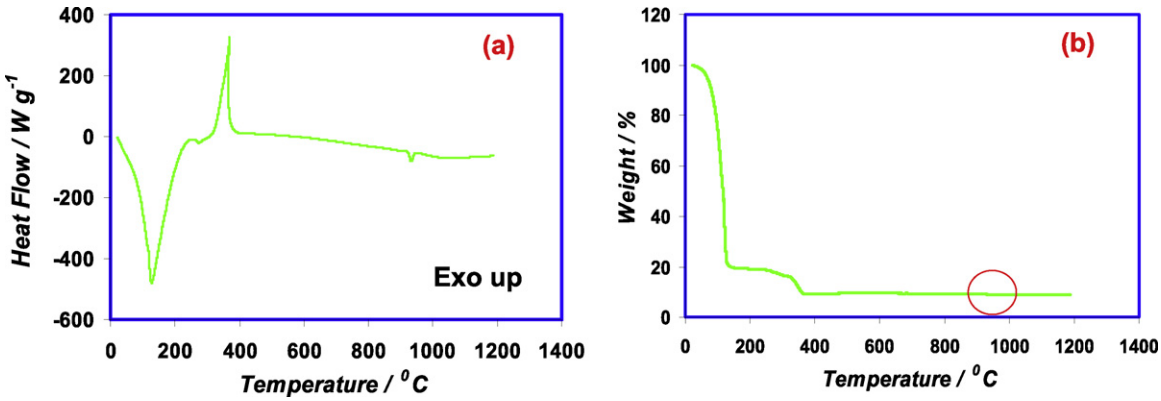

Fig. 5. Differential scanning calorimetry (DSC)–Thermogravimetry (TGA) analysis of solution precursor (a) DSC – heat flow curve and (b) TGA – weight change curve.

temperatures fall rapidly. The temperature of the substrate was measured to be around 350–365 °C throughout the deposition process, which is below 900 °C and because of this reason we expect conversion of CoO back into Co_3O_4 in the deposited coatings. On the other hand, it is also possible that the size of some of the droplets could also limit the high temperature conversion of Co_3O_4 into CoO in the plasma plume itself because of large thermal mass. The other possibilities could include incomplete conversion of the solution precursor droplets (in the plasma plume), and incomplete back conversion of CoO into Co_3O_4 due to rapid quenching after exiting the plasma plume. Therefore, one can expect to have Co_3O_4 phase in the as-deposited coatings along with a mixture of partially converted solution precursor phase (CATH), as well as quenched CoO phase. In the present study, the X-ray diffraction pattern of as-deposited Co_3O_4 film (see Fig. 4) did not indicate existence of CoO or unconverted CATH phases, which may be related to the detection limit of the X-ray diffraction technique. Therefore, to determine the existence of other phases and the thermal stability of the Co_3O_4 films, DSC–TGA scans were run on scraped powders of as-deposited films. For comparison purposes, DSC–TGA scans were run on commercial Co_3O_4 powders also, which are shown in Fig. 6. Commercial powders did not show any thermal reaction or change in the weight till ~870 °C, and the endothermic reaction with associated weight loss at this temperature could be attributed to conversion of Co_3O_4 into CoO phase. Similar behavior can be seen in the plasma deposited Co_3O_4 films also, except the low temperature weight loss till 400 °C. Also, the endothermic reaction temperature (~800 °C) in the plasma deposited coatings is slightly lower compared to the commercial powders, and this must be because of very fine particulate size of Co_3O_4 phase in the as-deposited films, which is shown in the microstructural analysis section. However, initial weight loss at low temperatures could be due to either incomplete conversion of the solution precursor or the quenched CoO phase in the as-deposited films. Partially converted CATH in the solution precursor should cause in weight loss with increasing the temperature, similar to the phase transitions shown in Fig. 5; however, a reverse conversion of CoO into Co_3O_4 should result in an exothermic reaction associated with a slight weight gain. There are no indications for an exothermic conversion of CoO into Co_3O_4 in the heat flow curve. Also, even if there are any undetectable minute thermal reactions taking place, it is yet difficult for exact quantification of contributions to the weight change because of the partially converted CATH or CoO, and it may not be possible from these examinations as they have opposite effects on the weight change. However, these studies clearly indicate a requirement for controlled optimization of plasma deposition process parameters to obtain full conversion of the solution precursor into Co_3O_4 phase.

3.2. Microstructural characterization

The surface microstructures of as-deposited Co_3O_4 films are shown in Fig. 3 at different magnifications. During the deposition process, the thermo-chemically converted particles in the plasma plume could melt partially/fully and fuse together into clusters because of very high temperatures of the plasma plume, and therefore, films could have agglomerates of fused particles. Due to the particulate nature, these films also exhibit porosity as shown in Fig. 3. The arrows show ligaments of the porous network structure. Usually, porosity of the electrode material provides large surface area and an easy access for the electrolyte, and thereby facilitates shuttling of Li ions between the electrodes. It also

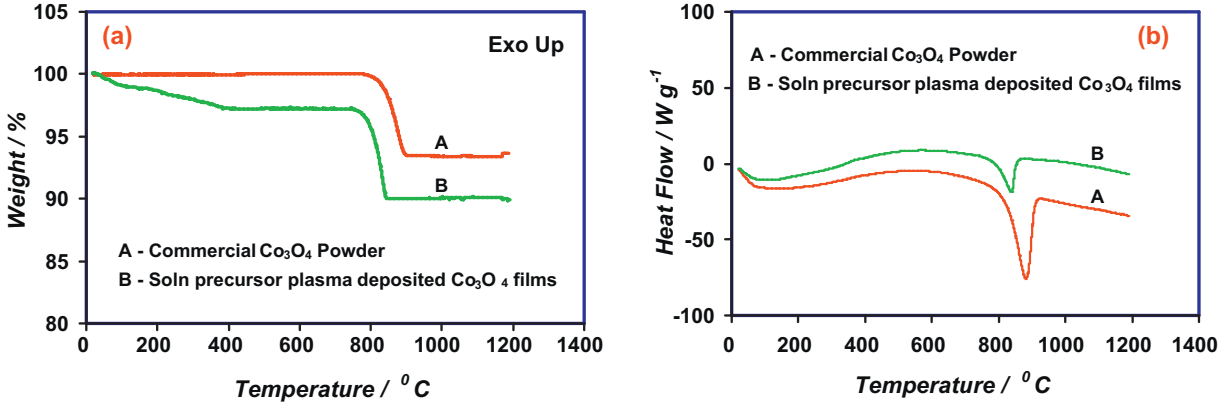

Fig. 6. Differential scanning calorimetry (DSC)–Thermogravimetry (TGA) analysis of solution precursor plasma deposited Co_3O_4 anode films.

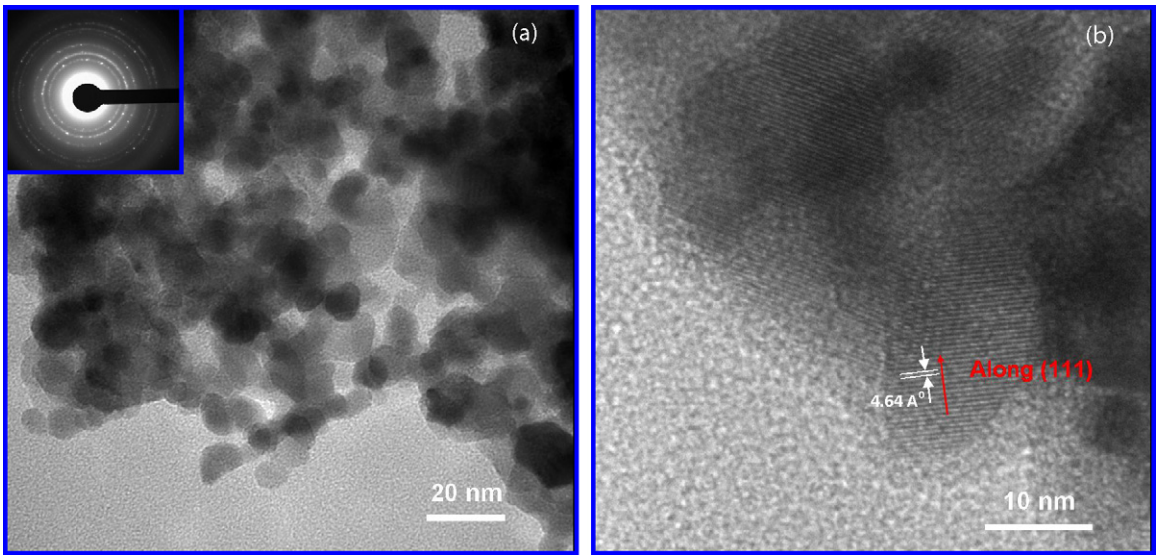

Fig. 7. Transmission electron microscopy images of Co_3O_4 anode film – (a) particulates of Co_3O_4 phase and the diffraction pattern is shown in the inset, and (b) high resolution lattice image of Co_3O_4 particulates.

accommodates the volume changes upon lithiation/delithiation of the electrode material during charge/discharge cycling process. Therefore, porous microstructures of the current Co_3O_4 anodes are very much desired for enhanced performance of Li-ion batteries. Fig. 7 shows the bulk microstructural analysis of Co_3O_4 films. Fig. 7(a) shows a high magnification TEM image of agglomerates of Co_3O_4 particulates, and these particulates must have been the resultant of thermo-chemical conversion of the solution precursor droplets. The size of these particles is in the range of 10–30 nm. Nanoparticles of the Co_3O_4 phase are also very important for better electrochemical performance as they provide large surface area with reduced mass and charge diffusion distances for rapid electrochemical reactions. Fig. 7(b) shows interplanar spacing between two consecutive (1 1 1) planes of Co_3O_4 crystal structure inside a particulate. The diffraction pattern in the inset of Fig. 7(a) and high resolution image in Fig. 7(b) also confirm the cubic phase of Co_3O_4.

3.3. Electrochemical characterization

Electrochemical characterization of the Co_3O_4 anode films was done without adding binder or carbon additive. The cyclic voltammetry (CV) studies performed between 0.05 and 3 V are shown in Fig. 8, and the scan rate employed was 0.05 mV s^{-1}. Out of the three CV cycles shown in Fig. 8, the first CV cycle shows anodic peaks at ~2.02 and 2.23 V and cathodic peaks at ~0.68 and 0.85 V. However, in the second cycle, there is a small shift in both the anodic and cathodic peaks. The anodic peaks shifted to 2.03 and 2.23 V, whereas the cathodic peaks shifted to 0.91 and 1.13 V, respectively, and these values remained same in the third and further cycles (not shown). The multi-step redox reactions of the Co_3O_4 phase as shown in the CV scans is because of multi-oxidation states of Co (Co^{2+} and Co^{3+}).

Fig. 9 shows the charge–discharge cycling of Co_3O_4 film tested at 0.15 C rate (1C = 890 mA gm^{-1}). The first cycle showed a discharge capacity of ~1007 mAhr g^{-1}, which is more than the theoretical capacity of Co_3O_4 and the first charge capacity was ~800 mAhr g^{-1}. However, in the subsequent cycles, the discharge and charge capacities were comparable with columbic efficiency around 100% or slightly above. The first discharge cycle showed a reduction plateau at ~1 V, similar to the voltages reported by other researchers for Co_3O_4 electrodes [11,29,38–40]. During the first discharge cycle, it

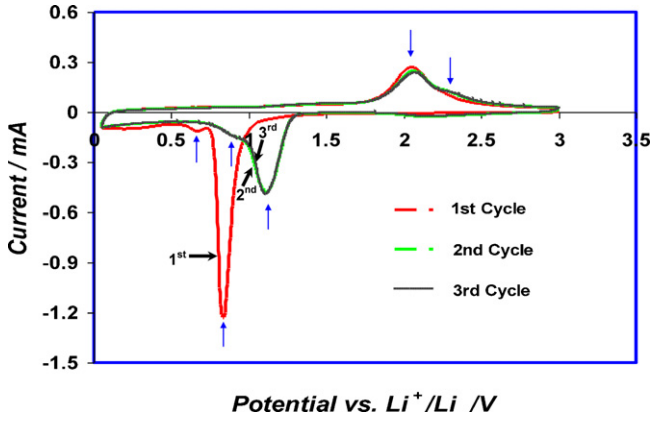

Fig. 8. Cyclic voltammograms (CVs) of solution precursor plasma deposited Co_3O_4 anode films (scanned at 0.05 mV s^{-1}).

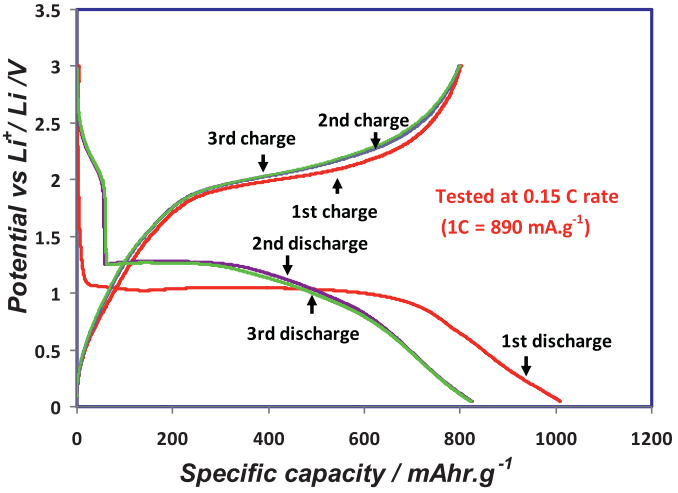

Fig. 9. Charge–discharge cycling of solution precursor plasma deposited Co_3O_4 anode at 0.15 C rate.

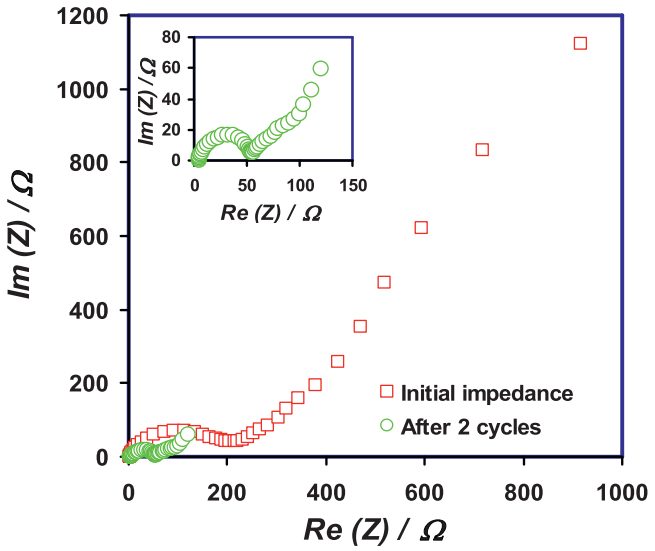

Fig. 10. Impedance of the Co_3O_4 anode (shown in Fig. 9) tested for three charge/discharge cycles (charge–discharge cycling was done at 0.15 C rate).

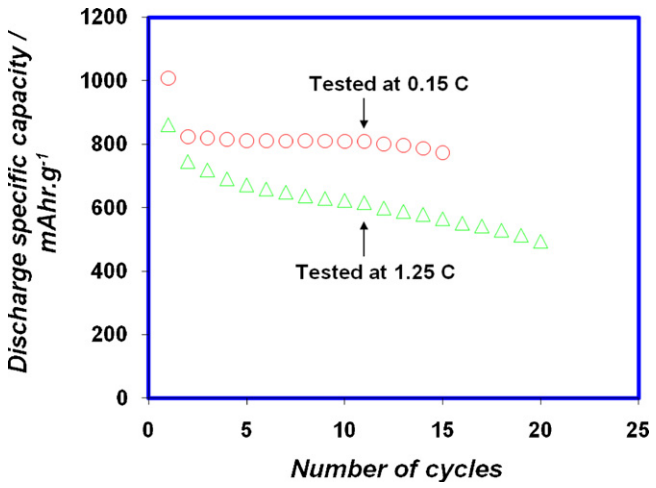

Fig. 12. Discharge specific capacities of solution precursor plasma deposited Co_3O_4 tested at different C rates for different number of charge/discharge cycles.

is expected that the Li ions react with Co_3O_4 phase to form Li_2O as shown in Eq. (1). In this process, Co_3O_4 phase is reduced to nano domains of metallic Co. In the subsequent cycles the voltage of the plateau increased to ~1.25 V, which is also in agreement with the literature [29,38–40]. However, in the second and third cycles, the discharge capacity was around 823 mAhr g^{-1}, which is lower than the initial discharge capacity observed. The reason for capacity loss could be due to conversion of Co into CoO phase, instead of Co_3O_4, during the charge processes, as pointed out earlier by several researchers [11,29,38–40]. At the same time, in the second and following discharge cycles, the CoO phase is expected to reduce to Co. We also examined impedance of the same cell before starting the discharge/charge cycles, as well as after the first two cycles, which are shown in Fig. 10. The initial impedance was very large and this could be due to improper wetting of the electrode by the electrolyte. With cycling of the cell, due to aging as well as continuous electrochemical interaction, the wetting of electrode must have improved the electrochemical characteristics of the cell and there by reduced the impedance. It is to be noted that, the impedance values reported in the literature are usually with combination of binder, conductive carbon, active material, along with other components of the cell. In the present case, absence of carbon may also have contributed to very high impedance of the cell. Fig. 11 shows the first and second discharge cycles and specific discharge capacities of the Co_3O_4 anodes tested at different C rates. It is apparent from Fig. 11(a) and (b) that the first discharge capacity is always higher than the second discharge capacity irrespective of the C rate employed, and this must be due to conversion of Co into CoO instead of Co_3O_4 in the second charge cycles. However, for a given cycle the voltage plateau kept on decreasing with increasing the C rate and this could be attributed to the internal resistance of the cell, because of which high currents always lead to overshoot in the voltage plateaus. In spite of this, the voltage plateaus shifted to higher values in the second discharge cycles, which is the typical characteristic of Co_3O_4 anode material. At high rate (16.5 C) testing also the anode material showed very high capacities around 571 (first cycle) and 467 mAhr g^{-1} (second cycle) and it is yet higher than the specific capacity of carbon anodes. Therefore, the solution precursor plasma deposited Co_3O_4 could also be used as an anode in high rate charging/discharging applications of Li-ion batteries. High discharge capacities at high C rates could be attributed to the nanostructures and porosity of the electrode material, which provide large amount of surface area with decreased diffusion distances to facilitate faster electrochemical kinetics during the charge/discharge processes. Fig. 12 shows the cyclability of solution precursor plasma deposited Co_3O_4 at different C rates. At 0.15 C rate, the discharge capacity was almost

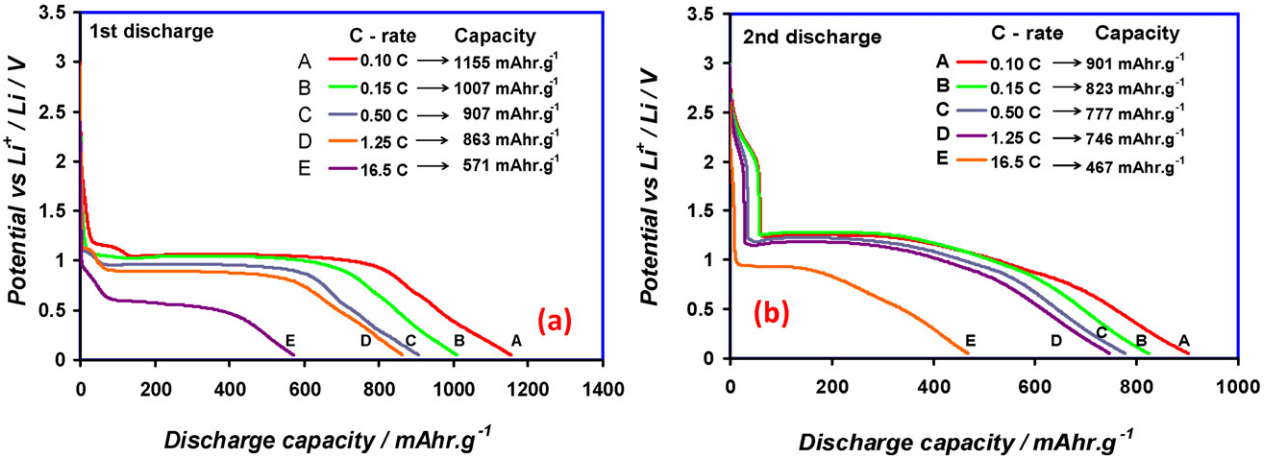

Fig. 11. (a) The first and (b) the second discharge cycles, and respective specific discharge capacities of solution precursor plasma deposited Co_3O_4 anodes tested at different C rates.

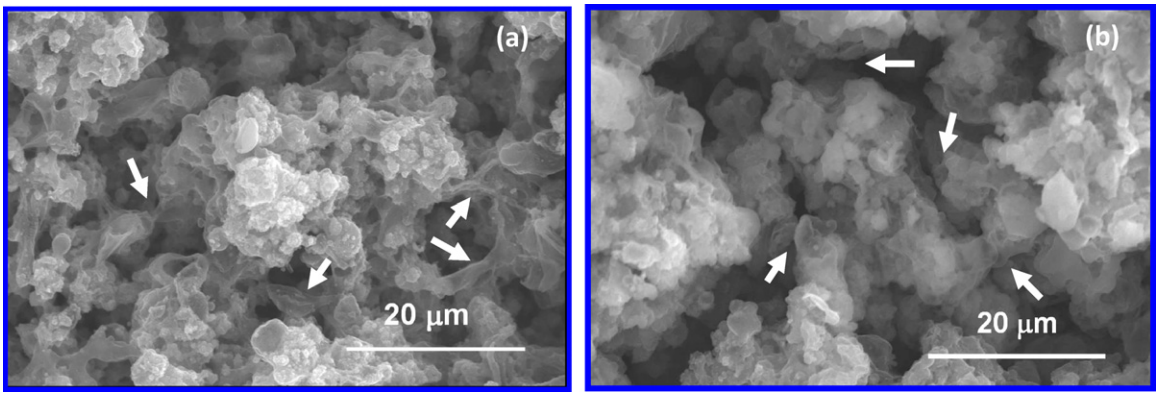

Fig. 13. SEM images of Co_3O_4 anodes (a) in the as-deposited condition: before testing electrochemically and (b) after testing for 20 cycles at a C rate of 1.25 C, and the arrows show presence of ligaments in (a) and broken or disappeared ligaments in (b).

constant from the second till the tenth cycle and then it started to decrease slowly with increasing the number of cycles. However, at 1.25 C rate, the discharge capacity decreased continuously with increasing the number of cycles. To determine the reason, we measured the impedance as well as examined the Co_3O_4 film tested at 1.25 C using SEM. The impedance was observed to increase (not shown here), and the SEM images shown in Fig. 13 also indicate disappearance of ligaments observed in the as-deposited films after twenty charge/discharge cycles of the electrode. Due to continuous cycling, the electrode material must have undergone fatigue because of volumetric expansion and contraction with the electrochemical reactions. Also, lack of cushioning effect due to the absence of carbon it may have affected the strain at interconnections and led to the broken ligaments. It is also possible that the broken or dislodged fine structures of the ligaments may have contaminated the electrolyte and thereby resulted in a fast decrease in the capacity. However, the sample tested at 1.25 C rate may have undergone rapid fatigue compared to the sample tested at 0.15 C rate and therefore led to a continuous decrease instead of a slow rate decrease in the capacity of the electrode. In addition, we expect some residual stresses in the as deposited Co_3O_4 films due to rapid cooling of the deposited material, and these may not have relieved after completion of the deposition process. Thus the strained structures of Co_3O_4 phase may not have sustained the volumetric expansion and contraction as easily as the strain free structures could do [8,41], and thereby resulted in broken structures. Therefore, addition of carbon and relieving of stresses in the as-deposited films by preheating the charge collector may help improve the cyclability of the electrodes. At this point, the role of residual or partially converted CATH on the cyclability is not known, but complete conversion of solution precursor or CATH into Co_3O_4 may certainly improve the capacity.

4. Summary

In summary, we have demonstrated successful processing of binder free, porous and nanostructured Co_3O_4 anodes directly on charge collectors with an industrial scale solution precursor plasma deposition technique. The nanostructures and porosity of the Co_3O_4 phase provide large surface area as well as reduced distances for ionic and charge transport during charge/discharge electrochemical reactions. DSC–TGA, X-ray diffraction and TEM examination confirm the cubic Co_3O_4 phase in the as-deposited material. However, optimization of plasma deposition in terms of atomization and a close temperature control of the process are required for a complete conversion of the solution precursor into Co_3O_4 phase. Electrochemical characterization indicated that the specific discharge capacities of solution precursor plasma deposited Co_3O_4 anodes could be close to the theoretical capacity. The first and second discharge cycles indicate a capacity loss due to possible conversion of Co_3O_4 into Co and then CoO in the subsequent discharge and charge cycles. Different C rate testing also confirms the above mentioned capacity loss and high rate testing indicates promising discharge capacity of the electrode. Cyclability data reveals that continuous volumetric expansion and contraction of the active material during charge/discharge cycling process may lead to fatigue of the material with lack of cushioning effect, and thus result in broken ligaments and reduced capacity with increasing the number of cycles. Addition of carbon and optimization of plasma deposition may be helpful to obtain long term cyclability. Thus the single stage solution precursor plasma deposition of Co_3O_4 directly on charge collector could be very economical for commercial production of batteries.

References

[1] C. Liu, F. Li, L.-P. Ma, H.-M. Cheng, Adv. Mater. 22 (2010) E28.
[2] M. Stanley Whittingham, Chem. Rev. 104 (2004) 4271.
[3] J.M. Tarascon, M. Armand, Nature 414 (2001) 360.
[4] Y. Takeda, M. Nishijima, M. Yamahata, K. Takeda, N. Imanishi, O. Yamamoto, Solid State Ionics 130 (2000) 61.
[5] Y. Idota, T. Kubota, A. Matsufuji, Y. Maekawa, T. Miyasaka, Science 276 (1997) 1395.
[6] K.D. Kepler, J.T. Vaughey, M.M. Thackeray, Electrochem. Solid State Lett. 7 (1999) 307.
[7] O. Mao, R.A. Dunlap, J.R. Dahn, J. Electrochem. Soc. 146 (1999) 405.
[8] W.-J. Zhang, J. Power Sources 196 (2011) 13.
[9] C.K. Chan, H. Peng, G. Liu, K. McIlwrath, X.F. Zhang, R.A. Huggins, Nat. Nanotech. 3 (2008) 31.
[10] I.A. Courtney, W.R. McKinnon, J.R. Dahn, J. Electrochem. Soc. 146 (1999) 59.
[11] P. Poizot, S. Laruelle, S. Grugeon, L. Dupont, J.M. Tarascon, Nature 407 (2000) 496.
[12] D. Barreca, M. Cruz-Yusta, A. Gasparotto, C. Maccato, J. Morales, A. Pozza, C. Sada, L. Sanchez, E. Tondello, J. Phys. Chem. C 114 (21) (2010) 10054.
[13] J.L. Gomez Camer, F. Martin, J. Morales, L. Sanchez, J. Electrochem. Soc. 155 (2008) A189.
[14] X.W. Lou, D. Deng, J.Y. Lee, J. Feng, L.A. Archer, Adv. Mater. 20 (2008) 258.
[15] F. Zhan, B. Geng, Y. Guo, Chem. Eur. J. 15 (2009) 6169.
[16] W.Y. Li, L.N. Xu, J. Chen, Adv. Funct. Mater. 15 (2005) 851.
[17] F. Tao, C. Gao, Z. Wen, Q. Wang, J. Li, Z. Xu, J. Solid State Chem. 182 (2009) 1055.
[18] J.S. Do, C.H. Weng, J. Power Sources 146 (2005) 482.
[19] Y.M. Kang, K.T. Kim, J.H. Kim, H.S. Kim, P.S. Lee, J.Y. Lee, H.K. Liu, S.X. Dou, J. Power Sources 133 (2004) 252.
[20] W. Yao, J. Yang, J. Wang, Y. Nuli, J. Electrochem. Soc. 155 (2008) A903.
[21] H. Zhang, J. Wu, C. Zhai, X. Ma, N. Du, J. Tu, D. Yang, Nanotechnology 19 (2008) 035711.
[22] Y. Liu, C. Mi, L. Su, X. Zhang, Electrochim. Acta 53 (2008) 2507.
[23] J. Jiang, J. Liu, R. Ding, X. Ji, Y. Hu, X. Li, A. Hu, F. Wu, Z. Zhu, X. Huang, J. Phys. Chem. C 114 (2010) 929.
[24] Y. Lu, Y. Wang, Y. Zou, Z. Jiao, B. Zhao, Y. He, M. Wu, Electrochem. Commun. 12 (2010) 101.
[25] G. Linda, C. Roy, 2000. Available from: www.transportation.anl.gov/pdfs/TA/149.pdf.
[26] K.T. Nam, D.W. Kim, P.J. Yoo, C.Y. Chiang, N. Meethong, P.T. Hammond, Y.M. Chiang, A.M. Belcher, Science 312 (2006) 885.

[27] N. Du., H. Zhang, Chen.F B., J. Wu, X. Ma, Z. Liu, Y. Zhang, D. Yang, X. Huang, J. Tu, Adv. Mater. 19 (2007) 4505.
[28] F. Li, Q.Q. Zou, Y.Y. Xia, J. Power Sources 177 (2008) 546.
[29] Y. Li, B. Tan, Y. Wu, Nano Lett. 8 (1) (2008) 265.
[30] G. Che, B.B. Lakshmi, E.R. Fisher, C.R. Martin, Nature 393 (1998) 346.
[31] P.L. Taberna, S. Mitra, P. Poizot, P. Simon, J.M. Tarascon, Nat. Mater. 5 (2006) 567.
[32] C.R. Sides, C.R. Martin, Adv. Mater. 17 (2005) 125.
[33] M.A. Mohamed, S.A. Halawy, M.M. Ebrahim, J. Therm. Anal. 41 (1994) 387.
[34] R.W. Grimes, A.N. Fitch, J. Mater. Chem. 1 (3) (1991) 461.
[35] T. Wanjun, C. Donghua, Chem. Pap. 61 (4) (2007) 329.
[36] J. Karthikeyan, C.C. Berndt, J. Tikkanen, J.Y. Wang, A.H. King, H. Herman, Nanostruct. Mat. 9 (1997) 137.
[37] L. Xie, X. Ma, E.H. Jordan, N.P. Padture, D.T. Xiao, M. Gell, Mater. Sci. Eng. A 362 (2003) 204.
[38] Z.W. Fu, Y. Wang, Y. Zhang, Q.Z. Qin, Solid State Ionics 170 (2004) 105.
[39] G. Binotto, D. Larcher, A.S. Prakash, R.H. Urbina, M.S. Hegde, J.M. Tarascon, Chem. Mater. 19 (2007) 3032.
[40] M.N. Obrovac, R.A. Dunlap, R.J. Sanderson, J.R. Dahn, J. Electrochem. Soc. 148 (2001) A576.
[41] T. Brezesinski, J. Wang, R. Senter, K. Brezesinski, B. Dunn, S.H. Tolbert, ACS Nano 2 (2010) 967.